Article

Parametric Study on Mooring System Design of Submerged Floating Tunnel under Extreme Wave and Seismic Excitation

Woo Chul Chung [1], Chungkuk Jin [2,*], MooHyun Kim [3] and Sewon Kim [4,*]

1   Division of Mechanical Engineering, Korea Maritime & Ocean University, Busan 49112, Republic of Korea; wcchung@kmou.ac.kr
2   Department of Ocean Engineering and Marine Sciences, Florida Institute of Technology, Melbourne, FL 32901, USA
3   Department of Ocean Engineering, Texas A&M University, College Station, TX 77843, USA; m-kim3@tamu.edu
4   School of Intelligent Mechatronics Engineering, Sejong University, Seoul 05006, Republic of Korea
*   Correspondence: cjin@fit.edu (C.J.); sewonkim@sejong.ac.kr (S.K.)

Abstract: This study proposes a mooring design strategy for a submerged floating tunnel (SFT) subject to extreme waves and earthquakes. Several critical design parameters, such as submerged depth and mooring station interval, are taken into account. As a target structure, a 700 m long SFT system with permanent stations at both ends, representing the fixed–fixed-end boundary condition, is established. To consider coupled dynamics between the tunnel and the mooring system with structural elasticity, an efficient time-domain simulation model is established. Three combinations of environmental conditions are considered: extreme wave only, extreme earthquake only, and both extreme earthquake and operating wave. First, to check the submerged-depth effect on the dynamic response of the SFT system, including mooring tension, two different submerged-depth (deep and shallow) types are simulated and analyzed. It is confirmed that the deep submerged-depth model (A-type) has an advantage under extreme wave conditions, whereas the shallow submerged-depth model (B-type) is equipped with better resistance when subject to an earthquake. Thus, the compromise submerged-depth model (C-type) is newly devised to enhance structural integrity under various environmental circumstances. Furthermore, a mooring station interval sensitivity test with the C-type is performed and demonstrates the integrity of the C-type.

Keywords: submerged floating tunnel (SFT); submerged depth; earthquake; mooring interval; mooring system design

1. Introduction

The submerged floating tunnel (SFT), which consists of the main tunnel and mooring/foundation systems for station-keeping capability, has been considered one of the best solutions among countries that have difficulties in installing ground transportation paths due to deep creeps, such as canals, bays, fjords, and rivers [1–5]. Despite the advantages that foundation work can be decreased compared with conventional bridges, that an optimal design can be safe against both waves and earthquakes due to a deeply submerged tunnel and the existence of a flexible mooring system, and that minimal interference of ship voyage can be achieved with a sufficient submerged depth, there is no report yet regarding the construction of SFTs in the world due to a lack of high-level safety evaluation [6]; the first construction was considered by the Norwegian Public Road Administration (NPRA) in 2017 to connect a fjord in Norway [7].

There have been feasibility investigations around the world; concept studies under various environmental conditions—such as waves, currents, tsunamis, and earthquakes—and with regard to numerous design factors—such as buoyancy-to-weight ratios (BWRs), submerged

depths, and span lengths—have to be conducted to provide strong confidence in future construction [5,8–11]. The dynamic characteristic of SFTs and the corresponding mooring system when subject to waves and earthquakes are recognized as critical design factors, so many researchers have conducted experiments and numerical simulations.

As for numerical studies, Long et al. [4] conducted a case study to investigate the effect of the BWR and mooring stiffness. The dynamic response of coupled SFTs and mooring systems under wave and earthquake conditions was carried out by Di Pilato et al. [3]. Dynamic and structural responses, such as displacements and internal force/stress, of SFTs under hydrodynamic and 3D seismic excitation were evaluated by Muhammad et al. [12]. Moreover, the dynamic and structural responses of SFTs that have a large tunnel under wave and seismic conditions were investigated by Jin and Kim [13]. A minimum submerged depth of 25–30 m to both avoid a collision with a ship or submarine and reduce wave excitation effects was suggested by Indridason [14]. Since the submerged tunnel and mooring lines have a long, slender, circular shape, the vortex-induced vibration (VIV) effect should be considered, and Chen et al. [9] investigated mooring VIV effects on the SFT dynamic response. Furthermore, Luoa et al. [15] conducted a parametric study with respect to cable density, length, pretension, and velocity distribution that affect fatigue damage to SFT cables. Dynamic responses under slack and snap effects with an inclined mooring system were carried out [6]. Kunisu et al. [16] focused on analyzing the dynamic behavior and mooring tension of different mooring types, while Kunisu [17] further investigated wave forces on SFTs of different shapes and sizes. Jin et al. [10] compared the dynamics and structural responses of SFTs obtained using the potential-flow-based discrete module beam method and the Morison approach to identify the applicability of the Morison formula in hydrodynamic force calculations for deeply submerged tunnels.

On the one hand, many experimental approaches have been reported so far. For example, Oh et al. [18] examined the impacts of mooring types, water depths, and BWRs on the global performance of floating structures. Seo et al. [19] compared their numerical simulation model with experiments to assess its accuracy. Li et al. [20] studied the pressure characteristics of different tunnel shapes with pressure sensors around SFTs. Yang et al. [21] conducted parametric studies with varying factors, such as BWRs, water depths, wave heights, inclination angles of mooring lines, and wave periods. In addition, Oh et al. [22] carried out a scaled-down experiment considering the BWR, water depth, and mooring line shape, and its experimental result was compared with a numerical simulation [5]. A large-scale SFT was tested under conditions of regular and irregular waves in a 3D wave tank, and technical challenges were presented by Chung et al. [23]. Comprehensive reviews on various aspects of SFT dynamics were presented by Zhang et al. [24] and Xu et al. [25].

The present study focuses on mooring design with respect to various system parameters in large-wave and -earthquake conditions. Mooring length, submerged depth, and mooring interval play a crucial role in mooring tension and are evaluated to prevent mooring failures under large mooring tension. Once one mooring line is filed, progressive failure is inevitable under large wave conditions and seismic excitation. While several studies proposed various mooring configurations and assessed each configuration's advantages and disadvantages [26,27], our study provides engineering procedures on how mooring systems can be designed in a systematic way to ensure safety under wave and seismic excitation. This study investigates the dynamic characteristics of an SFT system, including mooring tension subject to (1) an extreme wave, (2) an extreme earthquake, and (3) an extreme earthquake with waves under an operating condition as environmental loadings. The structure of the paper is as follows: Section 2 explains the numerical model, SFT configuration, and environmental conditions; Section 3 presents the results with respect to submerged depth/mooring length through a comparison between A-type (deeply submerged) and B-type (shallow submerged) tunnels; Section 4 presents C-type tunnels as a compromise model to improve global performance; Section 5 shows the results at different mooring intervals with C-type tunnels; and Section 6 presents the conclusions and future work.

2. Numerical Model

2.1. Configuration

The specifications of the SFT used in this study are summarized in Table 1. In this study, the main SFT was modeled as an equivalent circular cylinder having the same axial, bending, and torsional moments as a circular tunnel with inner compartments for simplicity in the dynamic response analysis. The clamped–clamped boundary condition at both ends was used to apply a permanent station effect; rigid towers were assumed to be located at both ends of the tunnel for air ventilation and the evacuation of people during emergencies. The BWR was fixed at 1.3, which was close to the optimum value based on a previous parametric study [28].

Table 1. Parameters of the main SFT.

Main Tunnel						
BWR	Length	OD	Bending Stiffness	Axial Stiffness	Young's Modulus	Minimum Submerged Depth
[-]	m	m	N-m^2	N	N/m^2	m
1.3	700	20	1.34×10^{14}	3.23×10^{12}	3.0×10^{10}	61.5

Each mooring station consisted of four mooring lines inclined 60° to the seabed, as shown in Figure 1. The outer long lines were employed straight to the seabed, whereas the inner short mooring lines were installed crossing each other to increase the overall station-keeping capability. The mooring design was proposed in Ref. [22]. Chain mooring lines were considered, and the properties of the mooring chain materials are summarized in Table 2. Large-diameter mooring lines were considered to accommodate large dynamic motions and the resultant mooring tension. In addition, a large number of mooring lines are necessary to accommodate large dynamic motions and the resulting mooring tension under storm conditions, although this is not an economical choice.
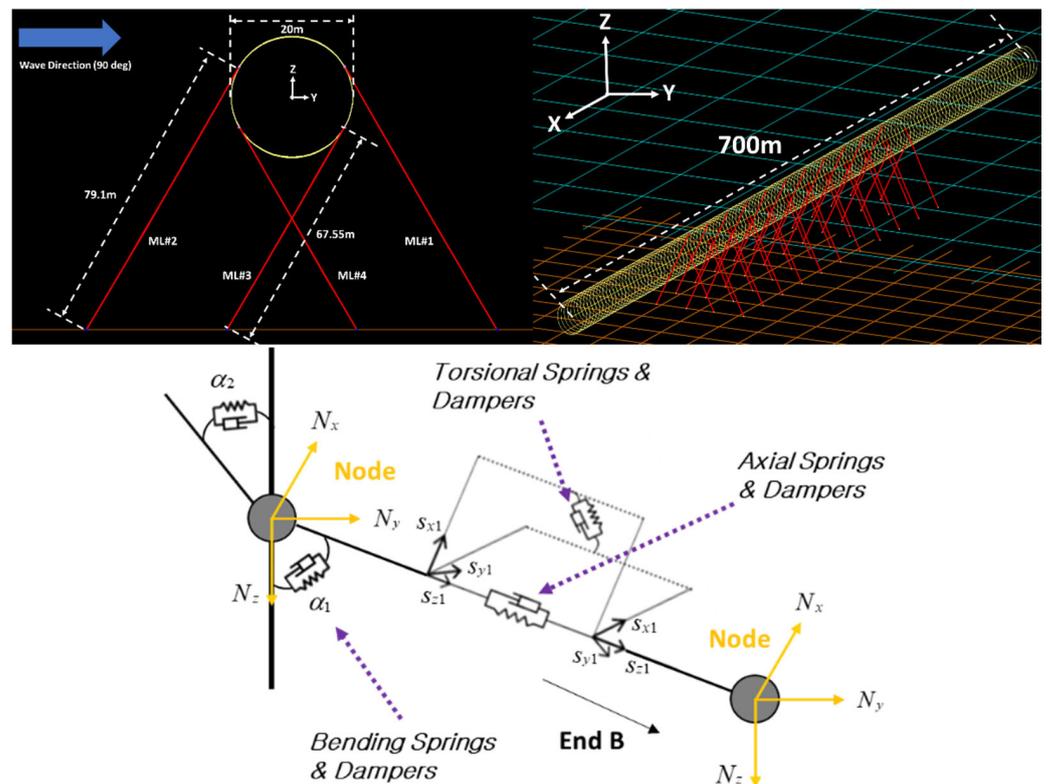
Figure 1. SFT mooring lines: arrangement (**Top**) and line model (**Bottom**).

Table 2. Properties of the mooring chain.

Mooring Chain Properties			
Bar Diameter	**Type**	**Density**	**Axial Stiffness**
m	**[-]**	**ton/m^3**	**N**
0.18	Studless Chain	0.645	2.77×10^9

2.2. Environmental Conditions

The environmental loading conditions are summarized in Table 3, and the corresponding time histories of the wave elevation and seismic motions are presented in Figure 2. First, an extreme wave condition with a 100 y return period in the Southern Sea of South Korea was considered. The JONSWAP wave spectrum, which is widely adapted for the offshore industry, was used as an input spectrum with a gamma value (enhancement parameter) based on average values in South Korea [28]. Random waves were generated by superposing 200 regular wave components with cutoff frequencies of 0.5 and 10 times the peak wave frequency. The equal energy method, in which each regular wave component has equal wave amplitude, is used to prevent long-time-history signals from being repeated by having different frequency intervals, $\Delta \omega$. Second, extreme seismic conditions with a 200 y return period for deep and soft ground (S5), with and without operating wave conditions, were considered simultaneously. The earthquake was generated by the response spectrum matching method using the wavelet algorithm suggested by Al Atik and Abrahamson [29] by modifying the earthquake measured in California with a moment magnitude of 6.8 provided by the U.S. Geological Survey. Other databases, such as the Pacific Earthquake Research Center and API standards, can also be employed [30,31].

Table 3. Environmental loading design conditions.

	Extreme Wave (100 Y Return)	Extreme Earthquake (200 Y Return)	Extreme Earthquake with Operating Wave
Hs(m)	11.70	[-]	2.00
Tp(s, rad/s)	13.0, 0.483	[-]	11.0, 0.571
Gamma	2.14	[-]	2.14
Earthquake	[-]	200 y S5	200 y S5

2.3. Time-domain Simulation

A fully coupled analysis tool is required to simulate the dynamic response of an SFT mooring system. OrcaFlex, a widely adapted commercial program in the offshore industry, was used [32]. In OrcaFlex, both the horizontal and vertical displacements of the main tunnel segment can be obtained by solving the following time-domain equation of motion (Equation (1)):

$$M\ddot{x}(t) + kx(t) = F_W(t) + F_M(t) + F_S, \tag{1}$$

where

M = Mass;
k = Total stiffness;
$F_W(t)$ = Hydrodynamic force;
$F_M(t)$ = Mooring force;
F_S = Static force (buoyancy $-$ weight);
$\ddot{x}(t)$ = Acceleration of themain tunnel;
$x(t)$ = Displacement of themain tunnel;
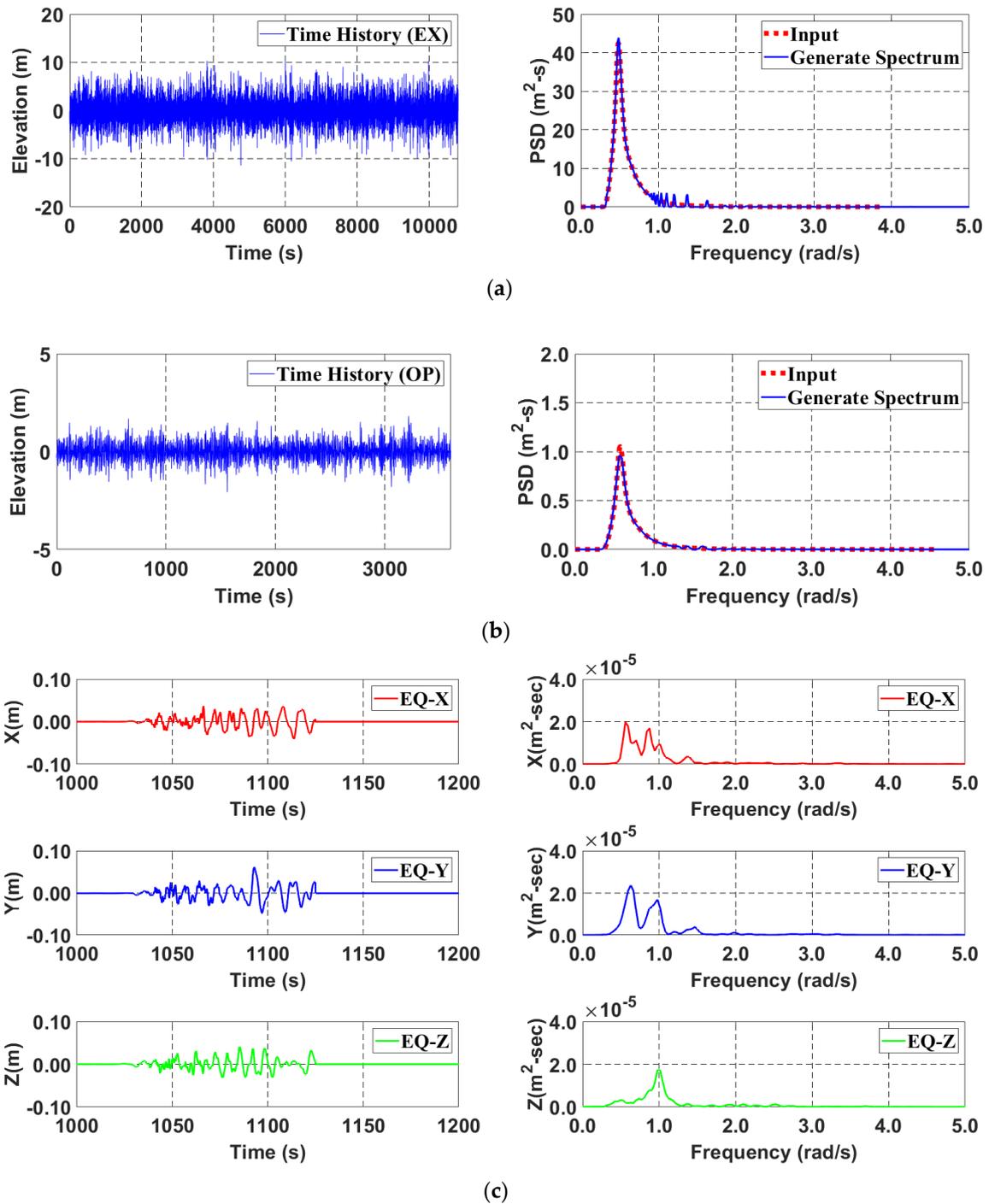
Figure 2. Time histories and spectra of the environmental conditions. (**a**) Time history (**left**) and spectra (**right**) of the 100 y extreme wave; (**b**) Time history (**left**) and spectra (**right**) of the wave in the operating conditions; (**c**) Time history (**left**) and spectra (**right**) of the seismic motion (200 y S5).

Generally, the Morison equation for a moving structure, consisting of a linear combination of inertia and drag terms (Equation (2)), is used to estimate the wave excitation loading of the structure. The Morison equation is typically used for a slender object with a wavelength five times larger than the cylinder diameter. In our study, some short-wavelength irregular waves did not satisfy this requirement. However, considering that, for deeply submerged tunnels, the amplitudes of high-frequency and low-wavelength waves rapidly

decay based on wave theory, using the Morison equation for force calculations is acceptable for the current tunnel model. The hydrodynamic force per unit length can be expressed as

$$F_W = \rho \cdot \frac{\pi D^2}{4} \cdot \ddot{\eta} - C_A \cdot \rho \cdot \frac{\pi D^2}{4} \cdot (\ddot{\eta} - \ddot{x}) + \frac{1}{2} \cdot \rho \cdot C_D \cdot D \cdot |\dot{\eta} - \dot{x}| \cdot (\dot{\eta} - \dot{x}), \quad (2)$$

where

C_A = Added mass coefficient;
C_D = Drag coefficient;
ρ = Seawater density;
D = Tunnel outer diameter;
$\dot{\eta}$ = Seawater velocity;
$\ddot{\eta}$ = Seawater acceleration;
$\dot{x}$ = Body velocity;
$\ddot{x}$ = Body acceleration.

In addition, the Wheeler stretching method was employed to estimate the wave-induced velocity and acceleration. Usually, in the linear wave theory (Airy wave theory), the horizontal wave-induced particle velocity can be expressed as follows (Equation (3)):

$$u(x, z, t) = \omega \varsigma_a \frac{\cosh[k(z + h)]}{\sinh(kh)} sin(\omega t - kx), \quad (3)$$

where

ω = wave frequency;
ς_a = wave amplitude;
k = wave number;
h = water depth;

The term $\cosh[k(z + h)] / \sinh(kh)$, which is a depth-oriented term, can decay exponentially according to the water depth. However, exaggerated values above the mean water level are expected. To mitigate this unrealistic value, the Wheeler stretching method can replace the original z with the suggested z/ (Equation (4)). Longridge et al. [33] observed that the Wheeler stretching method provides reasonable results in terms of wave kinematics compared with linear wave theory.

$$z'(x, t) = \frac{h(h + z)}{h + \varsigma(x, t)} - h \quad (4)$$

In the global performance simulation with OrcaFlex, the main tunnel and mooring line were modeled as lumped masses to represent structural elasticity. Each slender line was divided into several nodes and segments. Structural properties, such as mass, buoyancy, drag, and inertia, are lumped at nodes that are connected to each other with linear and rotational springs to present structural deformability, as shown in Figure 1 [32]. The torsional moment and motion of both the tunnel and mooring lines were not considered in this study because of their cylindrical shape and lowest torsional natural frequency, far outside the dominant frequency ranges of wave and earthquake excitations. The tunnel and mooring lines were coupled by a specially devised connection method called the dummy-connection-mass method [34], where 6-DOF dummy masses are placed whenever a connection between the tunnel and the mooring lines is needed. Dummy masses other than the connection medium did not affect the dynamics of the entire system.

The time histories of the seismic excitations were input at both ends of the tunnel and the anchor points of the mooring lines. Thus, seismic waves could propagate from the two ends of the tunnel to the mid-length through the tunnel and the anchor points of the mooring lines to the tunnel through the mooring lines.

A previous study supported the validity of the proposed method in that the lumped mass method with the Morison equation for modeling both the tunnel and mooring lines

produced comparable results to the higher-fidelity model, in which the tunnel was modeled by a potential theory-based method, whereas the mooring lines were modeled by the rod theory with the Morison equation [10]. The dynamics of a rigid tunnel module with mooring lines have also been validated against experimental results [5]. Furthermore, to validate the numerical model using OrcaFlex, an experiment was conducted at a 1:33.3 scale. It was also demonstrated that there is a correlation between the presented numerical model and the experimental results [23].

3. Effect of Submerged Depth

The submerged depth is a critical factor in the design of underwater structures. Based on Equation (2), the flow particle velocity and acceleration can be reduced exponentially as the water depth increases. Thus, the corresponding wave excitation force decays rapidly. Based on the submerged depth, the corresponding mooring line lengths also differ at a given water depth. As shown in Figure 3, in the deep submerged depth model (A-type), the mooring line length should be shorter than that in the shallow submerged depth model (B-type). Thus, the natural frequencies of the system also change owing to the different mooring line lengths. In addition, the trends and magnitudes of the dynamic responses and mooring tensions change owing to the stiffness variations. To evaluate the effect of the submerged depth, two environmental conditions, that is, extreme waves and earthquakes under waves in the operational condition, were considered with the simulation durations of 3 h and 1 h, respectively. In this study, a 700 m-span SFT with 11 mooring stations at 30 m intervals along the tunnel was employed at a water depth of 150 m. As the mooring interval was 30 m, the mooring line locations were concentrated around the mid-length. A water depth of 150 m was considered deep in the Southern Sea of South Korea. The submerged depth and corresponding mooring line length of each type, and the wet natural frequencies of the systems are listed in Tables 4 and 5, respectively. Because of its softer mooring system associated with the mooring length, the B-type tunnel has lower wet natural frequencies.
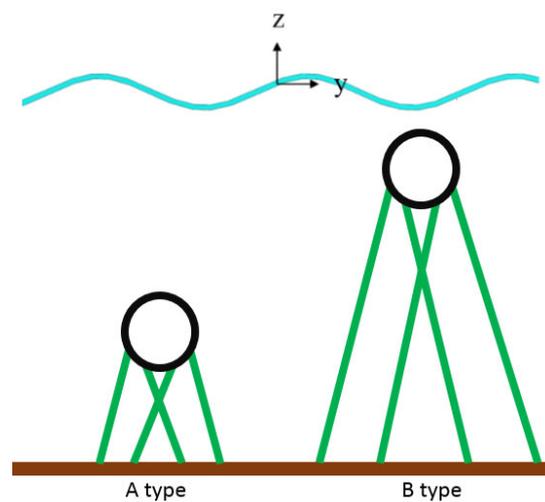
Figure 3. Configuration of the testing model for the effect of the submerged depth.

Table 4. Submerged depth and mooring line length in A-type and B-type tunnels.

Type	Submerged Depth	Mooring Line Length	
		Long	Short
	m	m	m
A-type	−111.5	50.23	38.68
B-type	−61.5	107.965	96.417

Table 5. Representative wet natural frequencies of A-type vs. B-type tunnels.

| Type | Wet Natural Frequency (rad/s) | | | |
| | Horizontal Mode | | Vertical Mode | |
	1st	2nd	1st	2nd
A-type	1.92	2.42	3.06	3.11
B-type	1.34	2.04	2.15	2.43

Figures 4 and 5 show the comparisons between the A- and B-type tunnels in terms of the horizontal time histories and their spectra. As shown in Figure 4, as expected, the horizontal motion of the B-type tunnel was much greater than that of the A-type tunnel under extreme wave conditions. This was primarily caused by the difference in the wave excitation forces owing to the change in the submerged depth. In addition, the B-type tunnel had lower wet natural frequencies closer to the dominant wave frequency than the A-type tunnel because it had longer mooring lines (i.e., lower mooring stiffness); therefore, the resonance effects were more pronounced in the B-type tunnel. The second peak of the B-type tunnel corresponded well with the first horizontal wet natural frequency, whereas the A-type tunnel had only one peak in the wave frequency region in the spectrum plot of Figure 4. With respect to earthquakes under the operating wave conditions presented in Figure 5, the B-type tunnel exhibited a relatively larger horizontal motion than the A-type tunnel. The 200 y earthquakes played an important role in horizontal motion, whereas the effect of wave excitations was smaller. With regard to wave excitations, the B-type tunnel had larger wave excitation owing to a shallower submerged depth. For earthquake excitations, the earthquake-induced resonance was more detectable in the B-type tunnel than in the A-type tunnel because of their natural frequency difference; the dominant earthquake frequency region was closer to the horizontal wet natural frequency in the B-type tunnel. In the spectrum plot, the first and second peaks of the B-type tunnel were located at the wave/earthquake excitation frequencies and the first horizontal wet natural frequency induced by earthquakes, respectively. The results for the A-type tunnel showed that there was only one peak at the first natural frequency induced by the earthquakes. Interestingly, a small peak value in the high-frequency region (approximately 3.8 rad/s) was confirmed in both types. This is related to the higher mode of the SFT system, which appears after a transient-like force owing to seismic motion. However, damping—the motion decay owing to energy dissipation—in the B-type tunnel was much greater than that in the A-type tunnel, as shown in Figure 5.
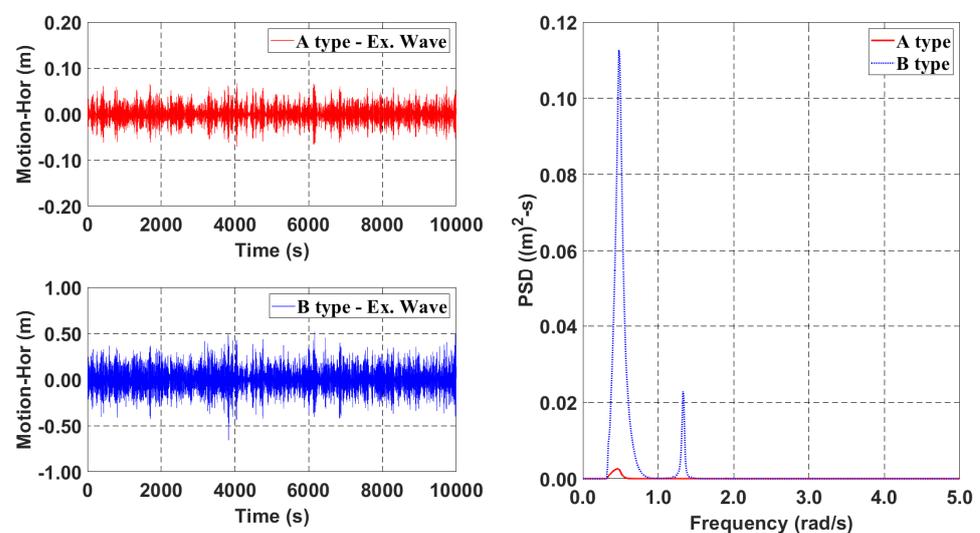
Figure 4. Time history and power spectral density (PSD) comparisons for the horizontal motion (A-type vs. B-type, extreme wave only).
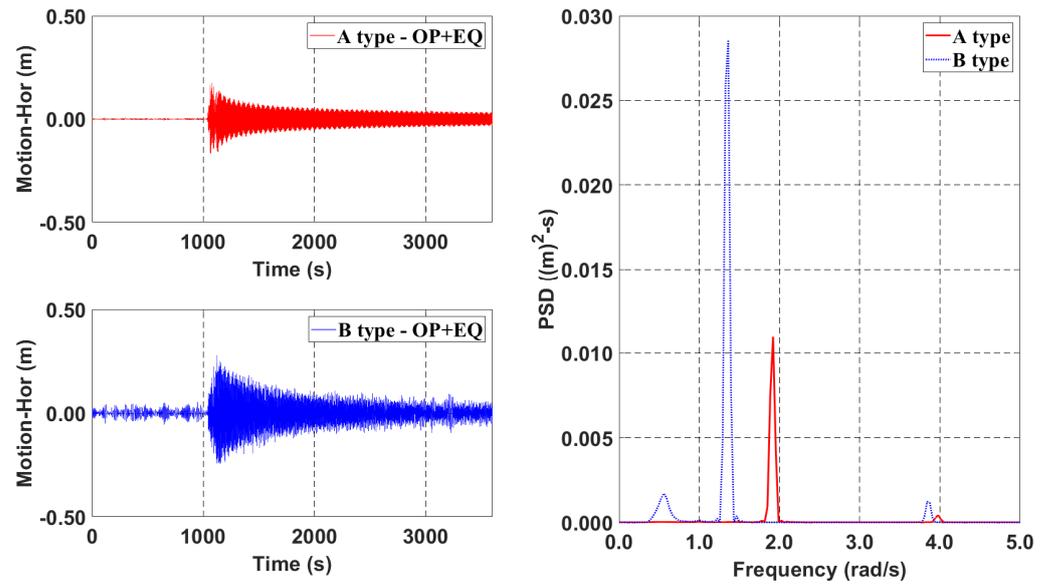
Figure 5. Time history and PSD comparisons for the horizontal motion (A-type vs. B-type, earthquake + operating wave).

The dynamic responses of the vertical motion are shown in Figures 6 and 7. For vertical motion, the B-type tunnel was more vulnerable than the A-type tunnel for both extreme wave excitation and earthquakes, which is supported by the simulation results. For the 100 y extreme wave case, a trend similar to that of the horizontal motion could be captured. The vertical dynamic response in the A-type tunnel was significantly smaller than that in the B-type tunnel owing to the reduction in the wave excitation force and the difference in the resonance effect. We also observed a similar trend in the case of a 200 y earthquake under operating wave conditions, as shown in Figure 7. The B-type tunnel resulted in higher vertical motion in terms of the maximum value in the time history plots and spectral area in the spectral plot, whereas vertical motion dissipation was faster in the B-type tunnel than in the A-type tunnel.
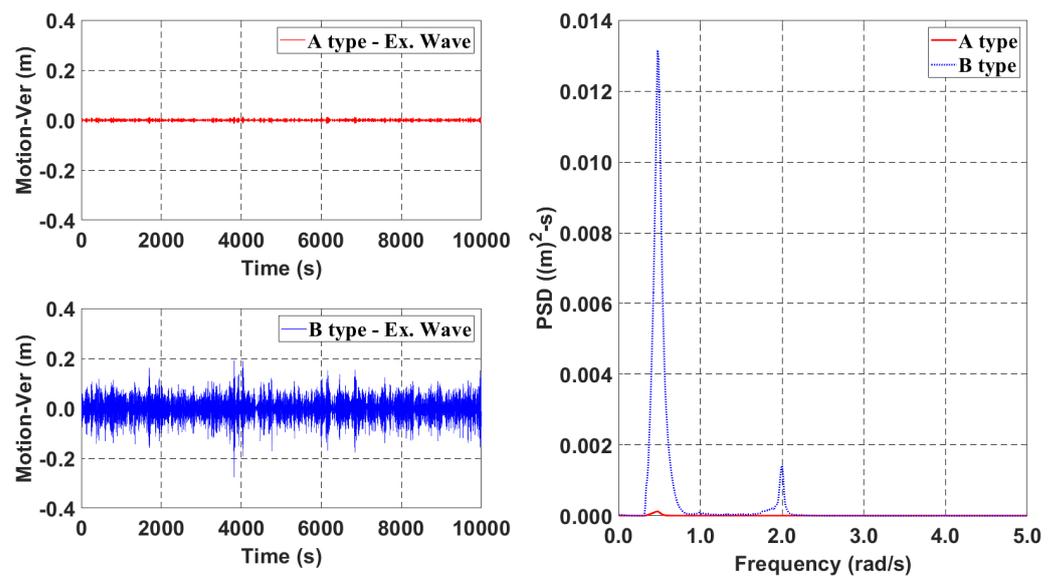
Figure 6. Time history and PSD comparisons for the vertical motion (A-type vs. B-type, extreme wave only).
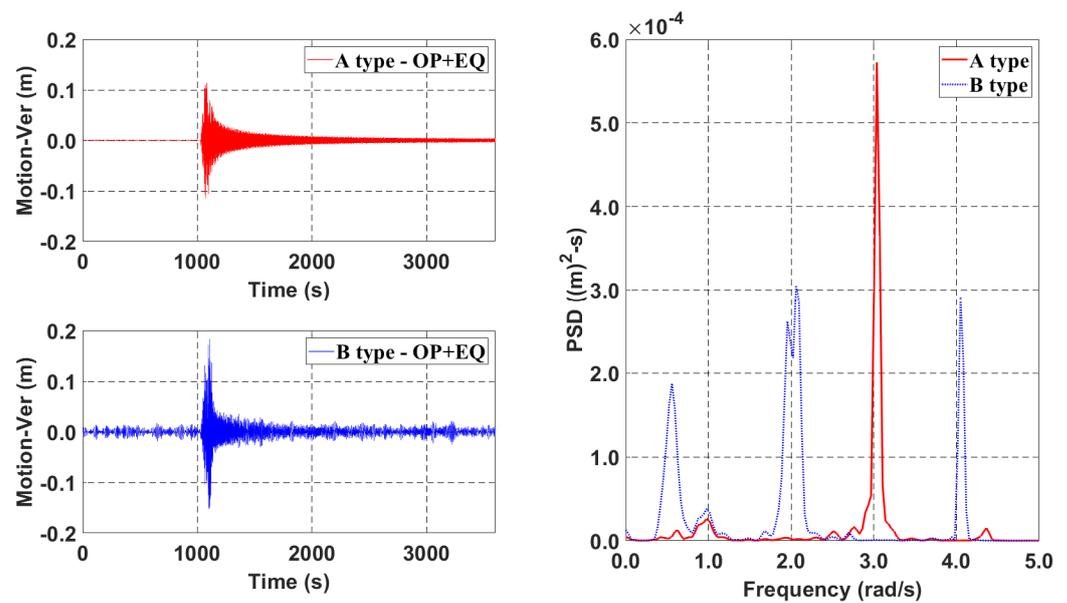
Figure 7. Time history and PSD comparisons for the vertical motion (A-type vs. B-type, earthquake + operating wave).

The corresponding mooring tensions for both types of tunnels are shown in Figures 8 and 9. Mooring tension is a critical parameter for determining structural safety. API Recommended Practice 2SK is typically applied to mooring safety evaluations. For intact mooring lines, the maximum mooring tension should be within the minimum breaking load, considering a safety factor of 1.67 for intact mooring lines. Owing to the environmental heading direction, only ML #3, which is the most critical line, is discussed in this and the following sections. As explained previously, with respect to the dynamic responses in the horizontal/vertical direction, the A-type tunnel is less vulnerable than the B-type tunnel under the extreme wave case. Thus, the mooring tension of the A-type tunnel was lower than that of the B-type tunnel. It was confirmed that the A-type tunnel has an advantage over the B-type tunnel under extreme wave conditions. However, even though the A-type tunnel had a smaller dynamic motion than the B-type tunnel under seismic excitations, the mooring tension in the A-type tunnel was much higher than that in the B-type tunnel. As the mooring line lengths in the A-type tunnel are shorter, small tunnel motions can result in large variations in the mooring tension. In other words, tension is a function of stiffness, such that $T = K_m \Delta x$, where $K_m = EA/L$ with EA representing the axial stiffness, L representing the mooring line length, and Δx representing the extension of the mooring line. Furthermore, as a shorter mooring line in the A-type tunnel has a higher K_m, a small value of tunnel displacement can result in high tension. Under extreme waves, the differences in the horizontal and vertical motions between the A- and B-type tunnels were large, which resulted in a higher dynamic mooring tension in the A-type tunnel than in the B-type tunnel. However, under a similar order of magnitude of motion under seismic excitation, the B-type tunnel was observed to be more beneficial because of the lower stiffness of the mooring lines, which caused a lower dynamic tension.
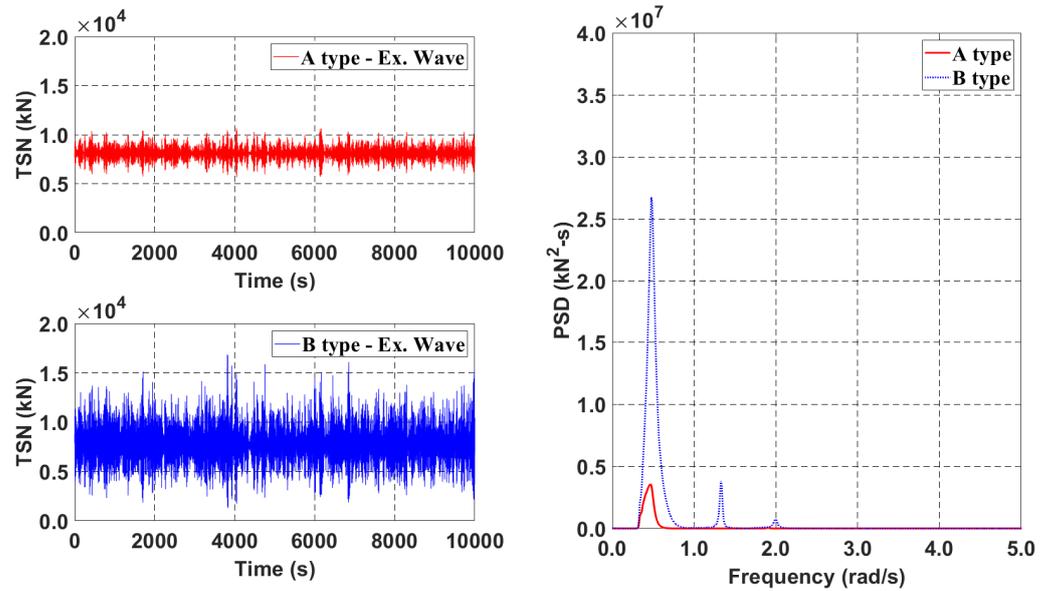
Figure 8. Time history and PSD comparisons of ML #3 (A-type vs. B-type, extreme wave only).
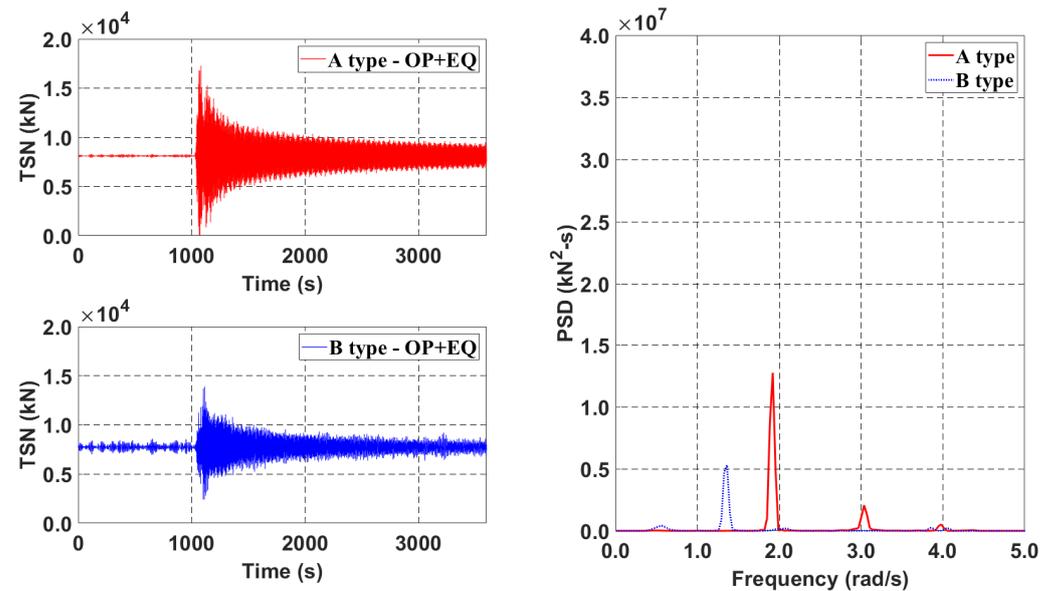
Figure 9. Time history and PSD comparisons of ML #3 (A-type vs. B-type, earthquake + operating wave).

4. Submerged-Depth Compromise Model (C-Type)

From the previous section, particularly with respect to mooring tension, it was observed that two different submerged-depth systems simultaneously have advantages and disadvantages in terms of extreme waves and earthquakes. Therefore, we introduced a compromised submerged-depth model (C-type) as a better SFT design by accommodating the advantages of both types while minimizing their disadvantages, as shown in Figure 10. Thus, a compromised submerged depth model (C-type) was used in the subsequent simulations. The submerged depth and corresponding mooring line length of the C-type tunnel are listed in Table 6.
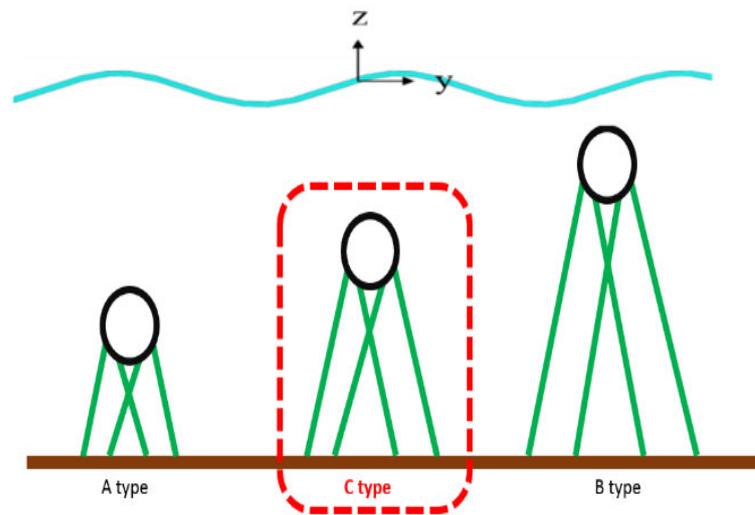
Figure 10. Schematic of compromised submerged-depth model (C-type).

Table 6. Submerged-depth/mooring line length, C-type.

	Submerged Depth	Mooring Line Length	
		Long	Short
	m	m	m
C-type	−86.5	79.097	67.550

5. Mooring Station Installation Interval Effect

As discussed in the previous sections, a compromised submerged-depth model (C-type) can be beneficial for improving global performance under both extreme waves and earthquakes. In addition, the interval of the mooring station, defined as a connection point between the tunnel and the mooring lines, can play a significant role in the dynamic response and mooring tension of the SFT system, as shown in Figure 11, which presents the configuration for the installation intervals of mooring lines in the longitudinal direction. In this regard, an additional parametric study with respect to the station intervals of the C-type tunnel is presented in this section. The same case studies were also performed for the A- and B-type tunnels. Statistical data at different mooring intervals for the A-, B-, and C-type tunnels are summarized in Appendix A. A comparison of the maximum mooring tension in Appendix A shows that the C-type tunnel can be a compromised model, which results in low levels of maximum mooring tension under both extreme waves and earthquakes. Therefore, in Section 5, the results for only the C-type tunnel are presented and discussed. In addition, to maintain consistency, the same environmental conditions (100 y extreme waves and 200 y earthquakes with operating waves) and the same number of mooring stations (11 stations) were applied to the compromised submerged depth model (C-type). Additionally, a case under earthquake excitations was tested to verify the influence of waves in the operating conditions on the overall dynamics. For the sensitivity test, dynamic simulations at the mooring station intervals of 30 m, 45 m, and 60 m were performed, and the tunnel length was fixed at 700 m. A 30 m interval indicates a concentrated arrangement around the mid-length, whereas a 60 m interval case shows a widely distributed mooring configuration along the length. The corresponding natural wet frequencies are listed in Table 7. The shorter the mooring station interval, the higher was the lowest horizontal/vertical wet natural frequency.
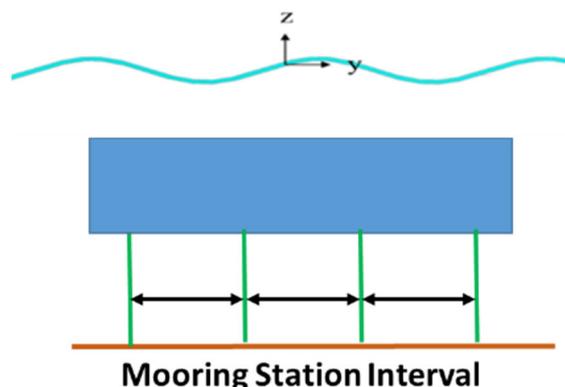
Figure 11. Configuration of the sensitivity test for the mooring station interval.

Table 7. Wet natural frequencies at different station intervals (C-type).

Station Interval (m)	Wet Natural Frequency (rad/s)			
	Horizontal		Vertical	
	1st	2nd	1st	2nd
30	1.55	2.24	2.43	2.70
45	1.39	2.26	2.19	2.77
60	1.27	2.19	1.95	2.62

The time histories and spectra of the horizontal motion under wave and earthquake excitations are shown in Figures 12 and 13, respectively. In the extreme wave case shown in Figure 12, the larger the mooring station interval, the greater the horizontal dynamic response. As the stiffness of the system at a longer station interval is lower, its behavior at the wave frequency region at approximately 0.5 rad/s is larger (first peaks). In addition, as shown in Table 7, the shorter the mooring station interval, the smaller the difference between the dominant wave frequency regions and the first wet natural frequency. Therefore, the resonance effect is more amplified for the case with a longer mooring station, as the second peaks are compared. Interestingly, for the earthquake case shown in Figure 13, the system with a 45 m station interval results in the largest horizontal response. As shown in Figure 2, among the three intervals, the case with a 45 m station interval has the highest seismic energy at the lowest horizontal wet natural frequency, which causes the largest motion. Under earthquakes, the natural frequency played an important role in the corresponding responses in our examples.

As shown in Figure 14, a trend similar to that in the horizontal direction under extreme waves could be captured for the vertical dynamic motion. The vertical motion is amplified as the station interval increases, owing to the resonance effect and lower system stiffness. On the other hand, Figure 15, which is the result of a 200 y earthquake with operational waves, shows that outstanding vertical motion could be captured from the 60 m interval system, whereas it could not occur in the 30 m and 45 m station interval systems. The resonance caused by a vertical earthquake in the 60 m station interval system could cause this outstanding peak value for the same reasons as in the horizontal motion under earthquakes. In both the horizontal and vertical motions, the operating waves have a negligible impact on the dynamics compared with the seismic excitations. This was confirmed by examining two earthquake cases: with and without operating waves. In particular, the spectral plots show negligible energy differences between the cases.
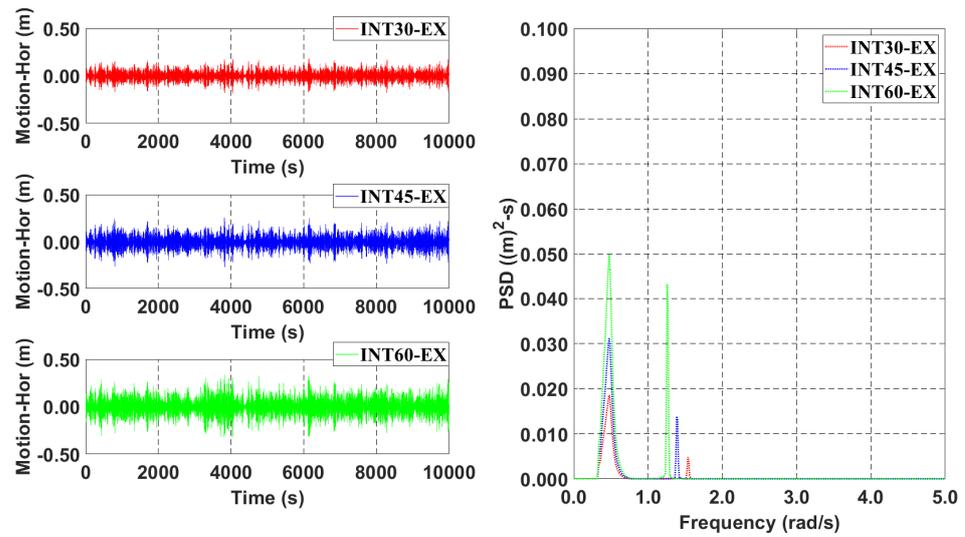
Figure 12. Time history and PSD comparisons for the horizontal motion at different station intervals (C-type, extreme wave only).
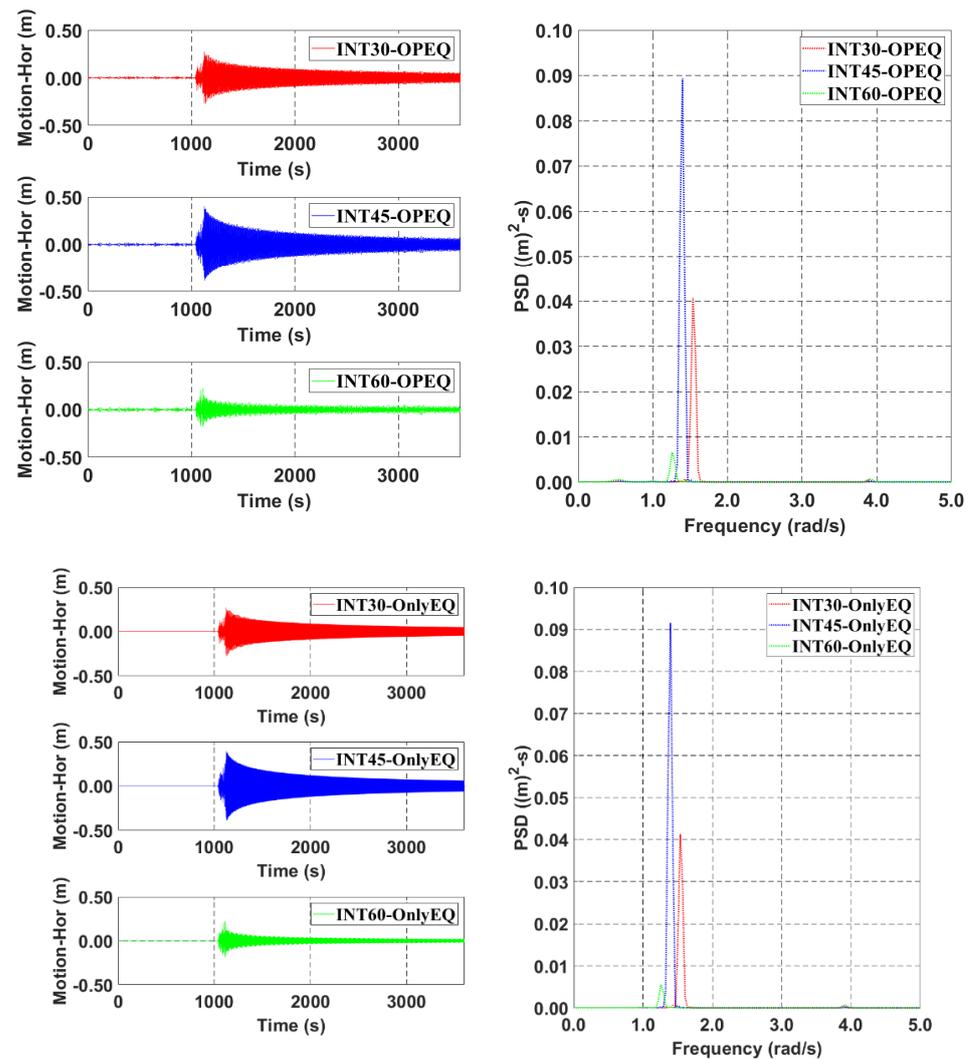
Figure 13. Time history and PSD comparisons for the horizontal motion at different station intervals (C-type, earthquake with operating wave (**Top**) and earthquake without operating wave (**Bottom**)).
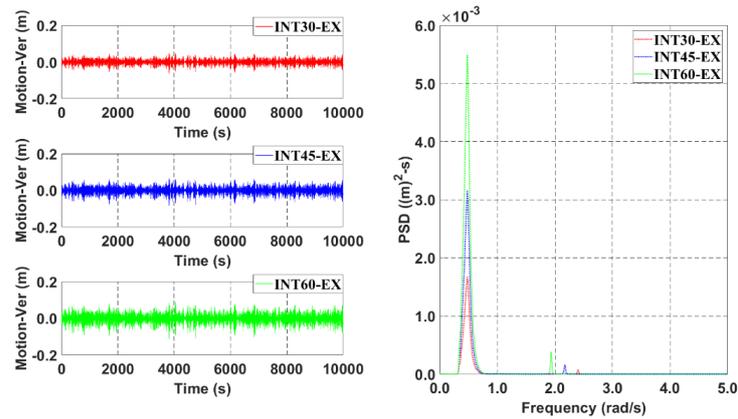
Figure 14. Time history and PSD comparisons for the vertical motion at different station intervals (C-type, extreme wave only).
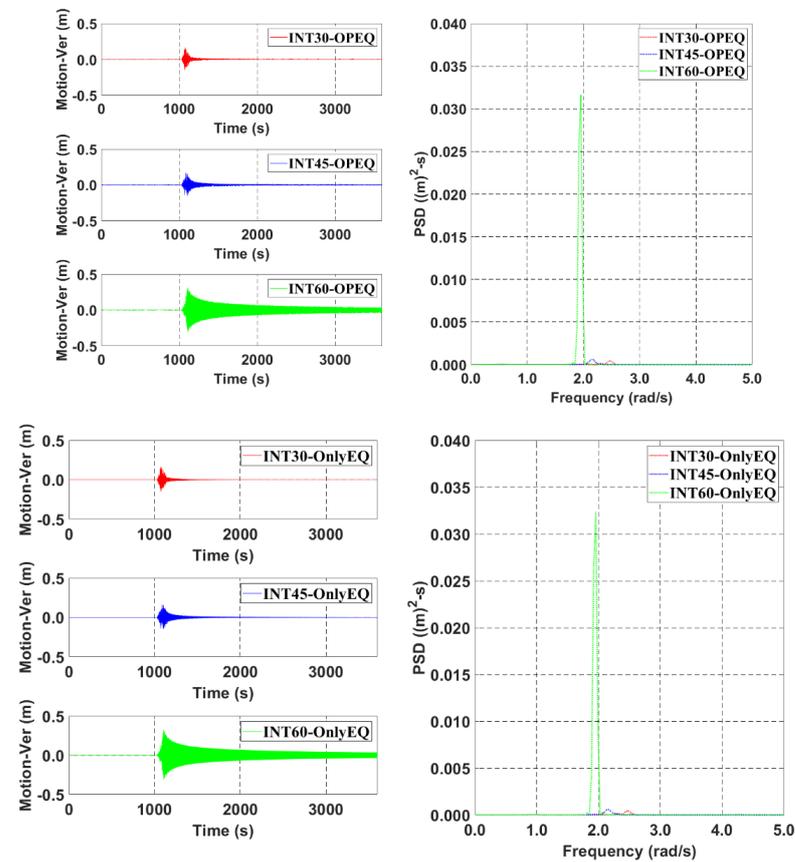
Figure 15. Time history and PSD comparisons for the vertical motion at different station intervals (C-type, earthquake with operating wave (**Top**) and earthquake without operating wave (**Bottom**)).

Finally, Figures 16 and 17 show the mooring tension in ML #3 under three different environmental loading conditions. In the extreme wave case, the dynamic mooring tension increased as the station interval was extended because both the horizontal and vertical motions were amplified. However, in the earthquake condition, the tension in ML #3 in the 45 m station interval system was mainly governed by the horizontal motion, whereas the vertical motion of the 60 m station interval system affected the corresponding mooring dynamic tension. Comparing the A-type and B-type tunnels with the C-type tunnel, when the station interval was 30 m, the C-type tunnel had the lowest mooring tension under both extreme wave and seismic excitations. In particular, the C-type tunnel resulted in a

much lower mooring tension under extreme seismic excitations, as indicated by the red line in Figure 9 (A-type), compared with the red line in Figure 17 (C-type at 30 m intervals). Therefore, our proposed compromise model (C-type) played an important role in mooring line safety under both extreme waves and earthquake excitations.
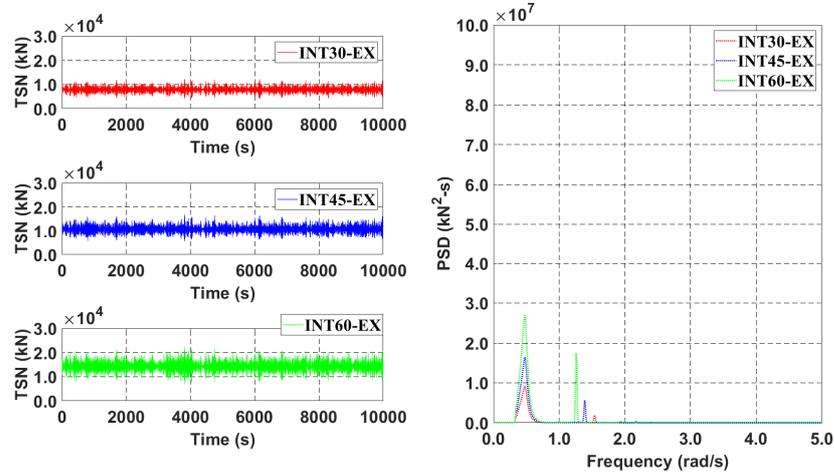
Figure 16. Time history and PSD comparisons of tension in ML #3 at different station intervals (C-type, extreme wave only).
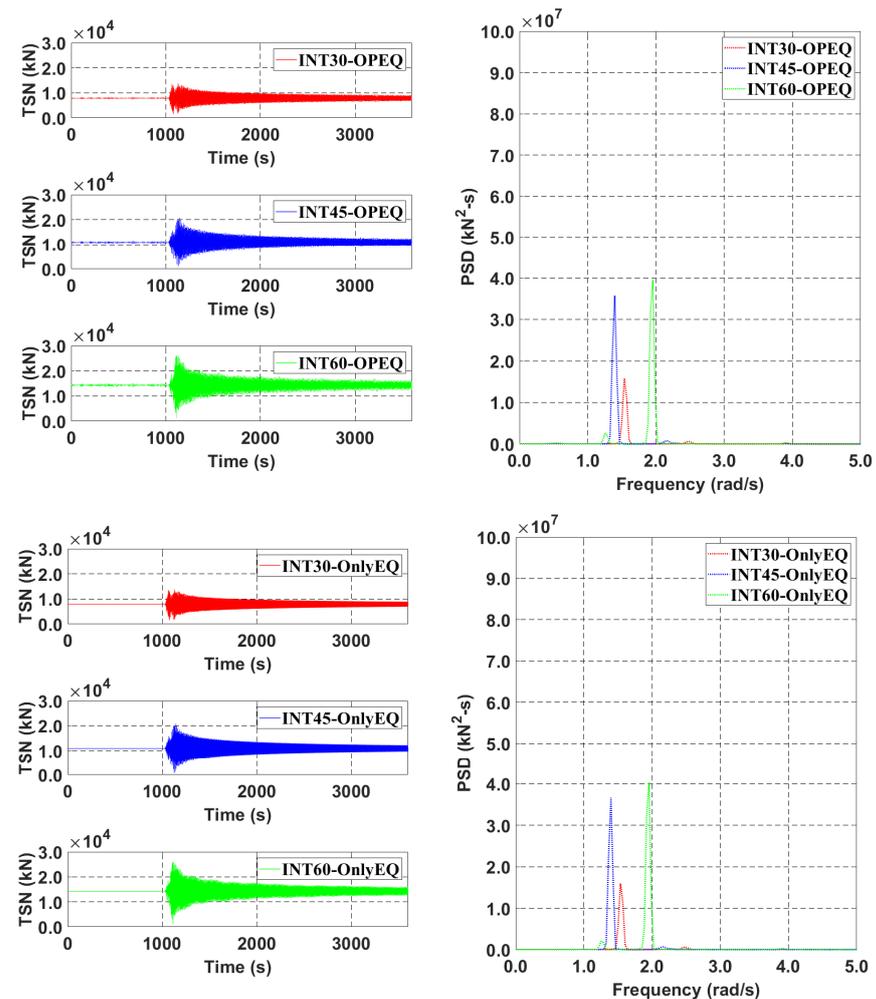
Figure 17. Time history and PSD comparisons of tension in ML #3 at different station intervals (C-type, earthquake with operating wave (**Top**) and earthquake without operating wave (**Bottom**)).

6. Conclusions

In this study, a numerical simulation of a 700 m-span SFT with rigid stations at both ends was conducted to check the effects of the submerged depth and mooring station interval on the dynamic response of the SFT system under extreme waves and earthquakes. This study was particularly focused on the mooring tension because it has been reported to be a serious factor in SFT design.

In terms of the effect of the submerged depth, the deep submerged depth model (A-type) has an advantage with respect to wave excitation loading because of the reduced wave loadings at deeper depths and a stiffer mooring system owing to shorter mooring lengths. In contrast, the shallow submerged depth model (B-type) also has an advantage during earthquakes because it has a long mooring line so that the mooring line can act as a damper to amplify the vibration energy dissipation, whereas the tension of the longer mooring is less sensitive to mooring extension because of lower stiffness.

The C-type model is proposed as a compromise to negotiate the advantages and disadvantages of each model simultaneously. Furthermore, a sensitivity test for the mooring station interval was conducted using the C-type model. The results showed that the longer the mooring interval, the greater the dynamic response under extreme wave excitations because of the lower natural frequency and stiffness caused by the station interval extension. However, under extreme earthquakes, the resonance at which the input earthquake frequency matches the wet natural frequency plays an important role in the SFT excitation and mooring tension. Thus, the 45 m station interval system has the largest horizontal dynamic motion, whereas the 60 m station interval system has the highest vertical motion. Thus, the corresponding mooring tension is governed by the dominant dynamic response of the SFT. Finally, the C-type tunnel at a station interval of 30 m could be a solution for resolving high mooring tension under extreme wave and seismic excitations. The given set of sensitivity tests demonstrated the importance of selecting an appropriate mooring interval and submerged depth under the given environmental conditions.

Appendix A Summary of Statistical Results

Appendix A summarizes the statistical results for both extreme waves and earthquakes with operating waves, as presented in Tables A1 and A2, respectively. Different mooring intervals of 30 m, 45 m, and 60 m were considered. The horizontal and vertical motions and mooring tensions were analyzed. The maximum and minimum values, mean values, and standard deviations were analyzed for the given cases.

Table A1. Summary of statistical results in extreme wave conditions.

Type	A-Type								
Mooring Interval	30 m			45 m			60 m		
Item	Horizontal Motion	Vertical Motion	ML #3 Tension	Horizontal Motion	Vertical Motion	ML #3 Tension	Horizontal Motion	Vertical Motion	ML #3 Tension
	m	m	kN	m	m	kN	m	m	kN
Max.	0.0671	0.0130	10,648.81	0.0904	0.0189	15,021.00	0.1185	0.0261	20,048.75
Min.	−0.0708	−0.0148	5656.23	−0.0962	−0.0221	8169.78	−0.1150	−0.0302	10,970.46
Mean	0.0000	−0.0001	8116.23	0.0000	−0.0001	11,656.58	0.0000	−0.0002	15,513.68
STD	0.0198	0.0040	721.84	0.0265	0.0058	984.79	0.0342	0.0077	1285.96
Type	B-Type								
Mooring Interval	30 m			45 m			60 m		
Item	Horizontal Motion	Vertical Motion	ML #3 Tension	Horizontal Motion	Vertical Motion	ML #3 Tension	Horizontal Motion	Vertical Motion	ML #3 Tension
	m	m	kN	m	m	kN	m	m	kN
Max.	0.5170	0.1906	16,870.94	0.7101	0.2311	22,733.26	0.8822	0.3042	28,495.34
Min.	−0.6537	−0.2738	1293.36	−0.7403	−0.3035	1409.34	−0.8073	−0.4087	2377.27
Mean	0.0000	0.0004	7779.55	0.0000	−0.0009	10,487.15	−0.0001	−0.0021	13,564.82
STD	0.1306	0.0443	2010.73	0.1693	0.0595	2741.02	0.2181	0.0786	3607.98
Type	C-Type								
Mooring Interval	30 m			45 m			60 m		
Item	Horizontal Motion	Vertical Motion	ML #3 Tension	Horizontal Motion	Vertical Motion	ML #3 Tension	Horizontal Motion	Vertical Motion	ML #3 Tension
	m	m	kN	m	m	kN	m	m	kN
Max.	0.1838	0.0490	12,189.47	0.2600	0.0671	16,919.03	0.3370	0.0863	22,249.23
Min.	−0.1848	−0.0624	4084.07	−0.2599	−0.0836	5458.68	−0.3247	−0.1115	7000.06
Mean	0.0000	−0.0003	7905.31	0.0000	−0.0005	10,927.20	0.0000	−0.0007	14,326.68
STD	0.0517	0.0147	1144.03	0.0685	0.0203	1548.11	0.0900	0.0268	2046.23

Table A2. Summary of statistical results in the extreme earthquake case with operating waves.

Type	A-Type								
Mooring Interval	30 m			45 m			60 m		
Item	Horizontal Motion	Vertical Motion	ML #3 Tension	Horizontal Motion	Vertical Motion	ML #3 Tension	Horizontal Motion	Vertical Motion	ML #3 Tension
	m	m	kN	m	m	kN	m	m	kN
Max.	0.1744	0.1133	17,291.76	0.1356	0.2544	24,629.90	0.2307	0.2660	31,509.47
Min.	−0.1701	−0.1153	10.21	−0.1345	−0.2273	16.15	−0.2341	−0.2530	21.59
Mean	0.0000	0.0001	8109.86	0.0000	0.0001	11,646.08	0.0000	0.0001	15,502.02
STD	0.0298	0.0085	1115.83	0.0140	0.0310	1959.88	0.0529	0.0318	2683.83

Table A2. *Cont.*

Type	B-Type								
Mooring Interval	30 m			45 m			60 m		
Item	Horizontal Motion	Vertical Motion	ML #3 Tension	Horizontal Motion	Vertical Motion	ML #3 Tension	Horizontal Motion	Vertical Motion	ML #3 Tension
	m	m	kN	m	m	kN	m	m	kN
Max.	0.2788	0.1836	13,895.45	0.2565	0.2163	16,056.17	0.3032	0.2734	21,351.29
Min.	−0.2455	−0.1517	2411.62	−0.2007	−0.1953	4141.90	−0.3425	−0.2503	4929.63
Mean	0.0000	0.0003	7739.02	0.0000	0.0001	10,438.30	0.0000	0.0001	13,494.08
STD	0.0523	0.0118	765.20	0.0375	0.0184	682.91	0.0413	0.0367	1068.40
Type	C-Type								
Mooring Interval	30 m			45 m			60 m		
Item	Horizontal Motion	Vertical Motion	ML #3 Tension	Horizontal Motion	Vertical Motion	ML #3 Tension	Horizontal Motion	Vertical Motion	ML #3 Tension
	m	m	kN	m	m	kN	m	m	kN
Max.	0.2738	0.1667	13,817.47	0.4022	0.1625	20,680.71	0.2229	0.3291	26,142.16
Min.	−0.2724	−0.1487	1501.24	−0.3877	−0.1502	812.12	−0.1812	−0.3119	1316.54
Mean	0.0000	0.0003	7890.84	0.0000	0.0002	10,905.37	0.0000	0.0002	14,296.01
STD	0.0559	0.0095	1142.12	0.0809	0.0113	1660.16	0.0263	0.0500	1838.12

References

1. Paik, I.Y.; Oh, C.K.; Kwon, J.S.; Chang, S.P. Analysis of wave force induced dynamic response of submerged floating tunnel. *KSCE J. Civ. Eng.* **2004**, *8*, 543–550. [CrossRef]
2. Ge, F.; Lu, W.; Wu, X.; Hong, Y. Fluid-structure interaction of submerged floating tunnel in wave field. *Procedia Eng.* **2010**, *4*, 263–271. [CrossRef]
3. Di Pilato, M.; Perotti, F.; Fogazzi, P. 3D dynamic response of submerged floating tunnels under seismic and hydrodynamic excitation. *Eng. Struct.* **2008**, *30*, 268–281. [CrossRef]
4. Long, X.; Ge, F.; Wang, L.; Hong, Y. Effects of fundamental structure parameters on dynamic responses of submerged floating tunnel under hydrodynamic loads. *Acta Mech. Sin.* **2009**, *25*, 335–344. [CrossRef]
5. Cifuentes, C.; Kim, S.; Kim, M.; Park, W. Numerical simulation of the coupled dynamic response of a submerged floating tunnel with mooring lines in regular waves. *Ocean Syst. Eng.* **2015**, *5*, 109–123. [CrossRef]
6. Lu, W.; Ge, F.; Wang, L.; Wu, X.; Hong, Y. On the slack phenomena and snap force in tethers of submerged floating tunnels under wave conditions. *Mar. Struct.* **2011**, *24*, 358–376. [CrossRef]
7. Ghimire, A.; Prakash, O. Intangible study for the design and construction of submerged floating tunnel. *Imp. J. Interdiscip. Res* **2017**, *3*, 721–724.
8. Deng, S.; Ren, H.; Xu, Y.; Fu, S.; Moan, T.; Gao, Z. Experimental study of vortex-induced vibration of a twin-tube submerged floating tunnel segment model. *J. Fluids Struct.* **2020**, *94*, 102908. [CrossRef]
9. Chen, Z.; Xiang, Y.; Lin, H.; Yang, Y. Coupled vibration analysis of submerged floating tunnel system in wave and current. *Appl. Sci.* **2018**, *8*, 1311. [CrossRef]
10. Jin, C.; Kim, G.-J.; Kim, S.-J.; Kim, M.; Kwak, H.-G. Discrete-module-beam-based hydro-elasticity simulations for moored submerged floating tunnel under regular and random wave excitations. *Eng. Struct.* **2023**, *275*, 115198. [CrossRef]
11. Marco, Z.; Giuseppe, C.P.; Giuseppe, T.; Marco, S. On the influence of shallow underground structures in the evaluation of the seismic signals. *Ing. Sismica* **2021**, *38*, 23–35.
12. Muhammad, N.; Ullah, Z.; Choi, D.-H. Performance evaluation of submerged floating tunnel subjected to hydrodynamic and seismic excitations. *Appl. Sci.* **2017**, *7*, 1122. [CrossRef]
13. Jin, C.; Kim, M. Dynamic and structural responses of a submerged floating tunnel under extreme wave conditions. *Ocean Syst. Eng.* **2017**, *7*, 413–433.
14. Indridason, B. *Earthquake Induced Behavior of Submerged Floating Tunnels with Tension Leg Anchorage*; Institutt for Konstruksjonsteknikk: Trondheim, Norway, 2013.

15. Luoa, G.; Chen, J.; Zhou, X. Effects of various factors on the VIV-induced fatigue damage in the cable of submerged floating tunnel. *Pol. Marit. Res.* **2015**, *22*, 76–83. [CrossRef]
16. Kunisu, H.; Mizuno, S.; Mizuno, Y.; Saeki, H. Study on submerged floating tunnel characteristics under the wave condition. In Proceedings of the Fourth International Offshore and Polar Engineering Conference, Osaka, Japan, 10–15 April 1994.
17. Kunisu, H. Evaluation of wave force acting on Submerged Floating Tunnels. *Procedia Eng.* **2010**, *4*, 99–105. [CrossRef]
18. Oh, S.-H.; Park, W.S.; Jang, S.-C.; Kim, D.H. Investigation on the behavioral and hydrodynamic characteristics of submerged floating tunnel based on regular wave experiments. *KSCE J. Civ. Environ. Eng. Res.* **2013**, *33*, 1887–1895. [CrossRef]
19. Seo, S.-i.; Mun, H.-s.; Lee, J.-h.; Kim, J.-h. Simplified analysis for estimation of the behavior of a submerged floating tunnel in waves and experimental verification. *Mar. Struct.* **2015**, *44*, 142–158. [CrossRef]
20. Li, Q.; Jiang, S.; Chen, X. Experiment on pressure characteristics of submerged floating tunnel with different section types under wave condition. *Pol. Marit. Res.* **2018**, *25*, 54–60. [CrossRef]
21. Yang, Z.; Li, J.; Zhang, H.; Yuan, C.; Yang, H. Experimental study on 2D motion characteristics of submerged floating tunnel in waves. *J. Mar. Sci. Eng.* **2020**, *8*, 123. [CrossRef]
22. Oh, S.-H.; Park, W.S.; Jang, S.-C.; Kim, D.H.; An, H.D. Physical experiments on the hydrodynamic response of submerged floating tunnel against the wave action. In Proceedings of the 7th International Conference on Asian and Pacific Coasts, APAC 2013, Bali, Indonesia, 24–26 September 2013; pp. 582–587.
23. Chung, W.C.; Jin, C.; Kim, M.; Hwang, J.-y. Comparison Study and Forensic Analysis between Experiment and Coupled Dynamics Simulation for Submerged Floating Tunnel Segment with Free Ends under Wave Excitations. *CMES-Comput. Model. Eng. Sci.* **2023**, *136*, 413–433. [CrossRef]
24. Zhang, H.; Yang, Z.; Li, J.; Yuan, C.; Xie, M.; Yang, H.; Yin, H. A global review for the hydrodynamic response investigation method of submerged floating tunnels. *Ocean Eng.* **2021**, *225*, 108825. [CrossRef]
25. Xu, W.; Ma, Y.; Liu, G.; Li, M.; Li, A.; Jia, M.; He, Z.; Du, Z. A review of research on tether-type submerged floating tunnels. *Appl. Ocean Res.* **2023**, *134*, 103525. [CrossRef]
26. Won, D.; Park, W.-S.; Kang, Y.J.; Kim, S. Dynamic behavior of the submerged floating tunnel moored by inclined tethers attached to fixed towers. *Ocean Eng.* **2021**, *237*, 109663. [CrossRef]
27. Fitriyah, D.K.; Suswanto, B.; Wahyuni, E. Analysis mooring system configuration of submerged floating tunnel. *IPTEK J. Proc. Series* **2017**, *3*, 116–119. [CrossRef]
28. Jin, C.; Kim, M. The effect of key design parameters on the global performance of submerged floating tunnel under target wave and earthquake excitations. *Comput. Model. Eng. Sci.* **2021**, *128*, 315–337. [CrossRef]
29. Al Atik, L.; Abrahamson, N. An improved method for nonstationary spectral matching. *Earthq. Spectra* **2010**, *26*, 601–617. [CrossRef]
30. Sun, Z.-Z.; Bi, C.-W.; Zhao, S.-X.; Dong, G.-H.; Yu, H.-F. Experimental analysis on dynamic responses of an electrical platform for an offshore wind farm under earthquake load. *J. Mar. Sci. Eng.* **2019**, *7*, 279. [CrossRef]
31. Zhao, S.-X.; Bi, C.-W.; Sun, Z.-Z. Engineering analysis of the dynamic characteristics of an electrical jacket platform of an offshore wind farm under seismic loads. *Appl. Ocean Res.* **2021**, *112*, 102692. [CrossRef]
32. Orcina, L. *OrcaFlex User Manual, Version 11.0 d*; Orcina: Ulverston, UK, 2020.
33. Longridge, J.; Randall, R.; Zhang, J. Comparison of experimental irregular water wave elevation and kinematic data with new hybrid wave model predictions. *Ocean Eng.* **1996**, *23*, 277–307. [CrossRef]
34. Jin, C.; Kim, M.-H. Time-domain hydro-elastic analysis of a SFT (submerged floating tunnel) with mooring lines under extreme wave and seismic excitations. *Appl. Sci.* **2018**, *8*, 2386. [CrossRef]